Articles

Epitaxial Electrodeposition of Tin(II) Sulfide Nanodisks on Single-Crystal Au(100)

Sansanee Boonsalee, Rakesh V. Gudavarthy, Eric W. Bohannan, and Jay A. Switzer*

Department of Chemistry and Graduate Center for Materials Research, Missouri University of Science and Technology, Rolla, Missouri 65409-1170

Received June 3, 2008. Revised Manuscript Received July 11, 2008

Epitaxial nanodisks of tin(II) sulfide (SnS) are deposited electrochemically on a [100]-oriented single-crystal Au substrate from an acidic solution at 70 °C. The SnS grows with two different out-of-plane orientations of [100] and [301], which each have four equivalent in-plane orientations. X-ray pole figures reveal the following epitaxial relationships: SnS(100)[010]//Au(100)[010], SnS(100)[010]//Au(100)[0$\bar{1}$0], SnS(100)[010]//Au(100)[001], SnS(100)[010]//Au(100)[00$\bar{1}$], SnS(301)[010]//Au(100)[010], SnS(301)[010]//Au(100)[0$\bar{1}$0], SnS(301)[010]//Au(100)[001], and SnS(301)[010]//Au(100)[00$\bar{1}$]. For the SnS[100] orientation, the in-plane mismatch is −2.4% in the [010] direction and 6.1% in the [001] direction. For the [301] orientation, the in-plane mismatch is −2.4% in the [010] direction and alternates between 3.4% and 6.7% in the [10$\bar{3}$] direction. The SnS deposits with a disklike morphology with a diameter of 300 nm and a thickness of 50 nm.

Introduction

Epitaxial films are typically deposited onto single-crystal substrates using vapor deposition. Recently, many research groups have utilized the electrochemical deposition method to produce epitaxial films.[1−6] The advantages of this method over other deposition methods are its versatility, high level of control, simplicity, and economy. The deposition is usually carried out at or near room temperature, which helps minimize solid-state diffusion between the film and substrate. The thickness of the film is easily controlled by the charge passed through the electrode. The electrochemical deposition method can be used to deposit materials on substrates of any shape or size. In addition, the departure from equilibrium is controlled through the applied overpotential, and the morphology of the deposits is often dependent on solution additives and the pH. Our group has previously employed electrodeposition in aqueous solution to grow epitaxial films of δ-Bi_2O_3,[7] Cu_2O,[6,8] CuO,[9] ZnO,[10,11] Fe_3O_4,[12] PbO_2,[13] Tl_2O_3,[14] and PbS[15] on single-crystal Au. We have also electrodeposited epitaxial Cu_2O films and nanostructures with tunable morphologies onto Si and InP single crystals.[16−18]

Tin sulfide (SnS) is a p-type layered semiconductor with a band gap ranging from 1.05 to 1.48 eV[19−22] depending on the preparation method, which is near the optimum energy band gap of 1.5 eV required for efficient light absorption for solar energy applications.[23] According to the recent study

* To whom correspondence should be addressed. Phone: (573) 341-4383. Fax: (573) 341-2071. E-mail: jswitzer@mst.edu.

(1) Pauporte, Th.; Cortes, R.; Froment, M.; Beaumont, B.; Lincot, D. *Chem. Mater.* **2002**, *14*, 4702.
(2) Froment, M.; Bernard, M. C.; Cortes, R.; Mokili, B.; Lincot, D. *J. Electrochem. Soc.* **1995**, *142*, 2642.
(3) Colletti, L. P.; Stickney, J. L. *J. Electrochem. Soc.* **1998**, *145*, 1442.
(4) Yang, F. Y.; Liu, K.; Hong, K.; Reich, D. H.; Searson, P. C.; Chien, C. L. *Science* **1999**, *284*, 1335.
(5) Mallett, J. J.; Svedberg, E. B.; Vaudin, M. D.; Bendersky, L. A.; Shapiro, A. J.; Moffat, T. P. *Phys. Rev. B* **2007**, *75*, 085304.
(6) Bohannan, E. W.; Shumsky, M. G.; Switzer, J. A. *Chem. Mater.* **1999**, *11*, 2289.
(7) Switzer, J. A.; Shumsky, M. G.; Bohannan, E. W. *Science* **1999**, *284*, 293.
(8) Switzer, J. A.; Kothari, H. M.; Bohannan, E. W. *J. Phys. Chem. B* **2002**, *106*, 4027.
(9) Switzer, J. A.; Kothari, H. M.; Poizot, P.; Nakanishi, S.; Bohannan, E. W. *Nature* **2003**, *425*, 490.
(10) Liu, R.; Vertegel, A. A.; Bohannan, E. W.; Sorenson, T. A.; Switzer, J. A. *Chem. Mater.* **2001**, *13*, 508.
(11) Limmer, S. J.; Kulp, E. A.; Switzer, J. A. *Langmuir* **2006**, *22*, 10535.
(12) Sorenson, T. A.; Morton, S. A.; Waddill, G. D.; Switzer, J. A. *J. Am. Chem. Soc.* **2002**, *124*, 7604.
(13) Vertegel, A. A.; Bohannan, E. W.; Shumsky, M. G.; Switzer, J. A. *J. Electrochem. Soc.* **2001**, *148*, C253.
(14) Vertegel, A. A.; Shumsky, M. G.; Switzer, J. A. *Electrochim. Acta* **2000**, *45*, 3233.
(15) Vertegel, A. A.; Shumsky, M. G.; Switzer, J. A. *Angew. Chem., Int. Ed.* **1999**, *38*, 3169.
(16) Switzer, J. A.; Liu, R.; Bohannan, E. W.; Ernst, F. *J. Phys. Chem. B* **2002**, *106*, 12369.
(17) Liu, R.; Bohannan, E. W.; Switzer, J. A.; Oba, F.; Ernst, F. *Appl. Phys. Lett.* **2003**, *83*, 1944.
(18) Liu, R.; Oba, F.; Bohannan, E. W.; Ernst, F.; Switzer, J. A. *Chem. Mater.* **2003**, *15*, 4882.
(19) Brownson, J. R. S.; Georges, C.; Lévy-Clément, C. *Chem. Mater.* **2006**, *18*, 6397. (a) Brownson, J. R. S.; Georges, C.; Lévy-Clément, C. *Chem. Mater.* **2007**, *19*, 3080.
(20) Brownson, J. R. S.; Georges, C.; Larramona, G.; Jacob, A.; Delatouche, B.; Lévy-Clément, C. *J. Electrochem. Soc.* **2008**, *155*, D40.
(21) Cheng, S.; Chen, G.; Chen, Y.; Huang, C. *Opt. Mater.* **2006**, *29*, 439.
(22) Cheng, S.; Chen, Y.; Huang, C.; Chen, G. *Thin Solid Films* **2006**, *500*, 96.
(23) Partain, L. D. *Solar Cells and Their Applications*; John Wiley & Sons: New York, 1995.

10.1021/cm801502m CCC: $40.75
Published on Web 08/22/2008

by Reddy and co-workers on the optical properties of SnS films, the optical band gap of SnS depends strongly on the lattice parameters.[24] Reddy et al. have fabricated p-SnS/n-CdS polycrystalline thin film cells with a solar conversion efficiency of 1.3%.[25] On the basis of the band gap of the material, a conversion efficiency of more than 25% is possible.[25,26] Additionally, Sn and S are inexpensive, environmentally benign, and ubiquitous in nature.[19,20,22] These properties make SnS suitable for use in photovoltaic and photoelectrochemical cells. SnS has been synthesized using many techniques including, for example, electrodeposition,[19−22,27,28] pulse deposition,[29,30] spray pyrolysis,[31,32] chemical vapor deposition,[33] and molecular beam epitaxy.[34]

Here, we show that epitaxial nanostructures of SnS can be electrodeposited onto single-crystal Au(100). The SnS was electrodeposited by the method developed by Brownson et al.[19] from a solution of $SnCl_2$, thiosulfate, and L-tartaric acid at pH 2.5. Our motivation for depositing epitaxial SnS on Au is 2-fold. First, we are interested in depositing high-aspect-ratio epitaxial deposits of the material for possible photoelectrochemical and photovoltaic applications. Electron−hole recombination should be minimized in the epitaxial structures because of the lack of grain boundaries in the direction perpendicular to the substrate. Also, the high aspect ratio should maximize collection of charge carriers. Recently, fabrication of high-aspect-ratio (length/diameter) semiconductors (Si, CdSe, CdTe) for photoelectrochemical and photovoltaic devices has attracted much attention compared with the conventional planar geometry.[35−38] The Lewis group has theoretically and experimentally shown that nanorod arrays of Cd(Se,Te) arranged perpendicular to the substrate enhance the overall efficiency. The design increases the charge carrier collection to the ultrathin p−n junction that is parallel to the substrate but orthogonal to the light absorption.[35,39] Our second motivation for studying this epitaxial system is that it provides fundamental information on the epitaxial growth of high-mismatch systems. δ-SnS has an orthorhombic structure ($a = 11.380$ Å, $b = 4.029$ Å, $c = 4.837$ Å),[20] whereas Au ($a = 4.079$ Å) has a face-centered cubic structure. We show in this work that mismatch is minimized when the SnS deposits with the a axis of SnS oriented perpendicular to the surface of the Au(100) substrate. The SnS nanostructures were characterized by X-ray diffraction, X-ray pole figures, and rocking curves. The film morphology was examined via scanning electron microscopy (SEM).

Experimental Section

SnS was deposited using the method developed by Brownson et al.[19] The deposition solution contained 50 mM $SnCl_2$, 150 mM $Na_2S_2O_3$ (sodium thiosulfate), 0.2 M L-tartaric acid, and 0.1 M HCl. The final pH of the solution was adjusted to 2.5 with 6 M NaOH. The bath temperature was maintained at 70 °C. When sodium thiosulfate was added to the solution, colloidal sulfur formed due to thiosulfate disproportionation. The cell consisted of a platinum counter electrode and a Ag/AgCl reference electrode. The working electrode was a crystal Au(100) single crystal purchased from Monocrystal Co. (diameter 10 mm, thickness 2 mm). A gold wire was wrapped around the single crystal to serve as an electrical contact. The Au(100) working electrode was placed in the solution using the meniscus method. Prior to deposition, the Au(100) single crystal was electropolished and annealed in a hydrogen flame. Electropolishing was performed at a constant anodic current density of 1.5 A/cm^2 in a solution containing 50 vol % ethanol, 25 vol % ethylene glycol, and 25 vol % concentrated HCl at 55 °C with a graphite counter electrode. The deposition solution was deaerated with Ar for 30 min prior to deposition to prevent the oxidation of Sn^{2+}. Argon gas was passed continually over the surface of the solution during deposition. The deposition was carried out in a fume hood. SnS films were deposited at a constant cathodic current density of 3 mA/cm^2 for 30 min with an EG&G Princeton Applied Research model 273A potentiostat/galvanostat.

X-ray diffraction (XRD) measurements were taken with a high-resolution Philips X'Pert diffractometer. The film XRD scan was obtained using Cu Kα_1 source radiation with a combination X-ray mirror and two-crystal Ge(220) two-bounce hybrid monochromator. The secondary optics module was a 0.18° parallel plate collimator. Rocking curves were run using a triple axis/rocking curve assembly as the secondary optics. The instrumental broadening is 25 arcseconds. Pole figures were run on the same instrument in point-focus mode using a crossed slit collimator as the primary optics and a flat graphite monochromator as the secondary optics. Stereographic projections were generated using CaRine Crystallography software (version 3.1). Interface models were generated using Cerius^2 1.0 software by Molecular Simulations. SEM images were taken with a Hitachi S-4700 cold field emission scanning electron microscope at an accelerating voltage of 5 keV.

Results and Discussion

The epitaxial deposition of SnS nanodisks is achieved by electrochemical reduction of $SnCl_2$ in the presence of $Na_2S_2O_3$ as a source of sulfur. The chemistry of tin monosulfide electrodeposition is described elsewhere.[20] The cathodic deposition current of 3 mA/cm^2 used in this study corresponds to a potential of approximately −0.45 V vs Ag/AgCl. This potential is 390 mV more positive than the potential of −0.86 V vs SCE reported by Brownson et al.[19] at the same current density, which is likely due to the higher electrical conductivity and catalytic activity of Au compared

(24) Reddy, N.; Koteeswara; Hahn, Y. B.; Devika, M.; Sumana, H. R.; Gunasekhar, K. R. *J. Appl. Phys.* **2007**, *101*, 093522.
(25) Ramakrishna Reddy, K. T.; Koteswara Reddy, N.; Miles, R. W. *Sol. Energy Mater. Sol. Cells* **2006**, *90*, 3041.
(26) Singh, J. P.; Bedi, R. K. *Thin Solid Films* **1991**, *199*, 9.
(27) Mishra, K.; Rajeshwar, K.; Weiss, A.; Murley, M.; Engelken, R. D.; Slayton, M.; McCloud, H. E. *J. Electrochem. Soc.* **1989**, *136*, 1915.
(28) Zainal, Z.; Hussein, M. Z.; Ghazali, A. *Sol. Energy Mater. Sol. Cells* **1996**, *40*, 347.
(29) Omoto, K.; Fathy, N.; Ichimura, M. *Jpn. J. Appl. Phys.* **2006**, *45*, 1500.
(30) Sato, N.; Ichimura, M.; Arai, E.; Yamazaki, Y. *Sol. Energy Mater. Sol. Cells* **2005**, *85*, 153.
(31) Lopez, S.; Ortiz, A. *Semicond. Sci. Technol.* **1994**, *9*, 2130.
(32) Reddy, N.; Koteeswara, Reddy; Ramakrishna, K. T. *Solid-State Electron.* **2005**, *49*, 902.
(33) Price, L. S; Parkin, I. P.; Hardy, A. M. E.; Clark, R. J. H.; Hibbert, T. G.; Molloy, K. C. *Chem. Mater.* **1999**, *11*, 1792.
(34) Nozaki, H.; Onoda, M.; Sekita, M.; Kosuda, K.; Wada, T. *J. Solid State Chem.* **2005**, *178*, 245.
(35) Kayes, B. M.; Atwater, H. A.; Lewis, N. S. *J. Appl. Phys.* **2005**, *97*, 114302.
(36) Green, M. A.; Wenham, S. R. *Appl. Phys. Lett.* **1994**, *65*, 2907.
(37) Tian, B.; Zheng, X.; Kempa, T. J.; Fang, Y.; Yu, N.; Yu, G.; Huang, J.; Lieber, C. M. *Nature* **2007**, *449*, 885.
(38) Tsakalakos, L.; Balch, J.; Fronheiser, J.; Korevaar, B. A.; Sulima, O.; Rand, J. *Appl. Phys. Lett.* **2007**, *91*, 233117/1.
(39) Spurgeon, J. M.; Atwater, H. A.; Lewis, N. S. *J. Phys. Chem. C* **2008**, *112*, 6186.

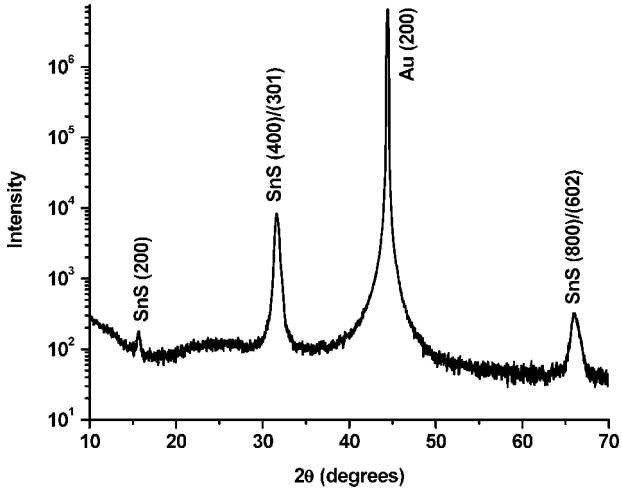

Figure 1. X-ray diffraction $\theta-2\theta$ scan probing the out-of-plane orientation of a SnS film electrodeposited on Au(100).

to the ITO. When a film is grown on a polycrystalline substrate such as stainless steel, the measured potential is −0.75 V vs Ag/AgCl.

The XRD $\theta-2\theta$ diffraction pattern of the SnS deposit on Au(100) is shown in Figure 1. Only three peaks are observed for SnS, which correspond well to the (200), (400), and (800) reflections of SnS. No other reflections are observed in the 2θ scan, indicating preferential [100] orientation of the film. Because only the $\{h00\}$-type reflection is observed in the diffraction pattern, only one lattice parameter can be determined (a = 11.31 Å). This value is similar to the a lattice parameter of the δ-SnS polymorph reported by Brownson et al. (a = 11.380 Å, b = 4.029 Å, c = 4.837 Å).[20] However, when a polycrystalline SnS is deposited on stainless steel using the same bath condition, the lattice parameters are a = 11.22 Å, b = 3.989 Å, and c = 4.328 Å. The lattice parameters obtained from the polycrystalline deposit are quite similar to the literature values of α-SnS (a = 11.18 Å, b = 3.982 Å, c = 4.329 Å, JCPDS no. 73-1859).[40] When the SnS(210) pole figure was run to determine the in-plane orientation of the film relative to the substrate, two different reflections that correspond to the [100] and [301] orientations were observed. Pole figures are obtained by choosing a specific plane to probe while measuring the diffracted intensity as a function of the tilt (χ) and rotation (φ). The (210) pole figure of the SnS is shown in Figure 2A, and the (111) pole figure of Au(100) is shown in Figure 2B. The radial grid lines in the pole figures correspond to 30° increments in χ. The SnS pole figure exhibits four equally spaced ($\Delta\varphi$ = 90°) peaks at χ = 54°, which is in agreement with the calculated χ = 54.5° that corresponds to the angle between the (210) and (100) planes in SnS. The other eight peaks at χ = 64° agree well with the calculated χ = 63.9°, corresponding to the angle between the (210) and (301) planes. The average peak height in Figure 2A is 360 counts/s for the (100) reflections and 76 counts/s for the (301) reflections, which indicates that the SnS deposit has a majority [100] orientation. The XRD diffraction pattern

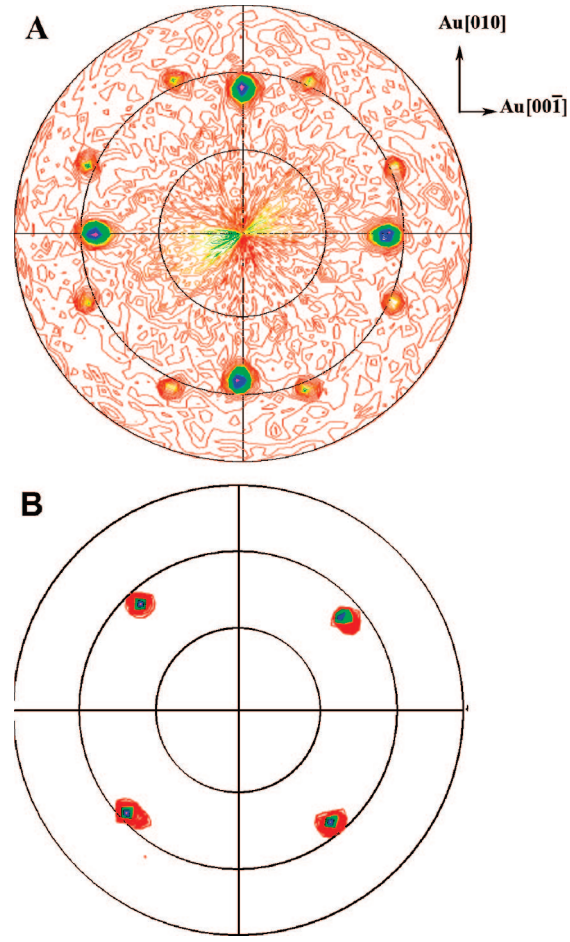

Figure 2. X-ray pole figures of (A) the SnS film and (B) Au(100). In (A), the four spots at χ = 54° correspond to the angles between the (210) and (200) planes, and the eight spots at χ = 64° correspond to the angles between the (210) and (301) planes. In (B), the four spots at χ = 54°correspond to the angle between the (111) and (100) planes of Au. The radial grid lines in the pole figures correspond to 30° increments in χ.

only shows three peaks because the (400) and (301) reflections overlap ($2\theta_{400}$ = 31.995° and $2\theta_{301}$ = 31.655°).

To help verify the assignment of in-plane orientations from the pole figure, stereographic projections were generated (Figure 3). The stereographic projections in Figure 3 are constructed using the orthorhombic α-SnS structure, because the atomic positions for the α-SnS structure are well-known and because δ-SnS is a slightly distorted structure of α-SnS.[20] Parts A and B of Figure 3 show the (100) and (301) stereographic projections, respectively, of orthorhombic α-SnS while probing the (210)-type reflections. In Figure 3A, the spots at χ = 54.5° are assigned to the {210} reflections due to the [100] orientation. Similarly, the spots at χ = 63.9° correspond to the {210} reflections in Figure 3B due to the [301] orientation. Parts A and B of Figure 3 are the resulting stereographic projections, assuming that only one domain of each orientation is deposited. However, the Au(100) substrate has 4-fold symmetry, so it is reasonable to expect four domains of each orientation being deposited on the surface. Overlaying parts A and B of Figure 3 on top of each other and then rotating the image by 90°, 180°, and 270° results in the stereographic projection shown in Figure 3C. The stereographic projection matches the experimentally observed pole figure shown in Figure 2A. The Au(111) pole

(40) del Bucchia, S.; Jumas, J. C.; Maurin, M. *Acta Crytallogr.* **1981**, *37B*, 1903.

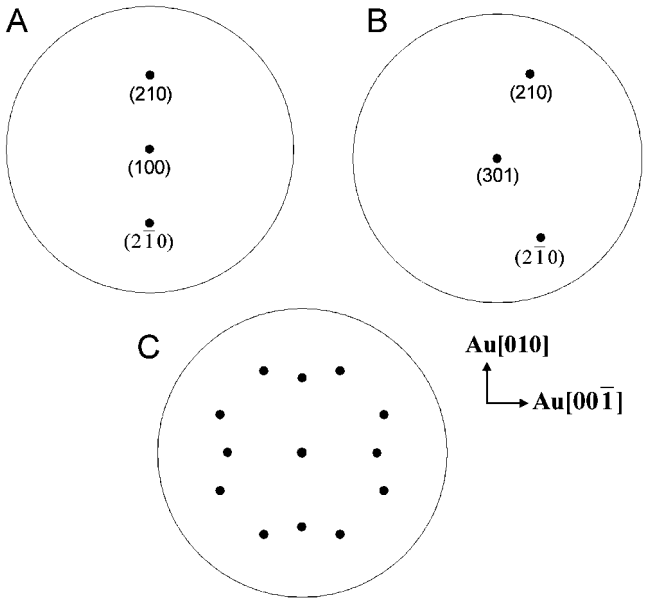

Figure 3. Stereographic projections for the (A) SnS[100] and (B) SnS[301] orientations indicating the positions where the (210)-type reflections should be observed in the pole figure. (C) Expected (210) pole figure for four domains obtained by overlaying the stereographic projections for the two orientations in (A) and (B) and rotating by 90°, 180°, and 270°.

figure in Figure 2B has four equally spaced peaks at $\chi = 55°$, which is consistent with the angle between the (111) and (100) planes in the cubic system. By comparing the two pole figures with the calculated stereographic projections, the in-plane orientation of SnS on Au is determined. The epitaxial relationships can be expressed as SnS(100)[010]//Au(100)[010], SnS(100)[010]//Au(100)[0$\bar{1}$0], SnS(100)[010]//Au(100)[001], SnS(100)[010]//Au(100)[00$\bar{1}$], SnS(301)[010]//Au(100)[010], SnS(301)[010]//Au(100)[0$\bar{1}$0], SnS(301)[010]//Au(100)[001], and SnS(301)[010]//Au(100)[00$\bar{1}$].

The SnS structure can be described as layers of double planes.[19,20,41] Each plane consists of Sn−S bonds arranged in zigzag chains that are parallel to the substrate (perpendicular to the *a* axis).[19] A unit cell of the SnS structure is shown in Figure 4. Tin atoms are colored blue, and S atoms are colored red. The (301) planes are shown in Figure 4 for reference. Interface models are shown in Figures 5 and 6 that are consistent with the epitaxial relationships determined from the X-ray pole figures. In the interface models, Au atoms are colored yellow and S atoms are colored red. For the SnS[100] orientation shown in Figure 5, the spacing between adjacent sulfur atoms is 3.982 Å along the *b* axis and 4.329 Å along the *c* axis. By comparing the spacings between sulfur atoms and Au atoms (4.079 Å), the lattice mismatch is calculated to be −2.4% in the [010] in-plane direction and 6.1% in the [001] in-plane direction. Hence, the system minimizes the lattice mismatch by placing the larger *a* lattice parameter (11.380 Å) perpendicular to the substrate. The *b* (4.029 Å) and *c* (4.837 Å) lattice parameters are similar to each other, and they are closer in value to the lattice parameter (4.079 Å) of the Au substrate. For the SnS[301] orientation shown in Figure 6, the (301) plane is also aligned with the Au. The distance between two sulfur

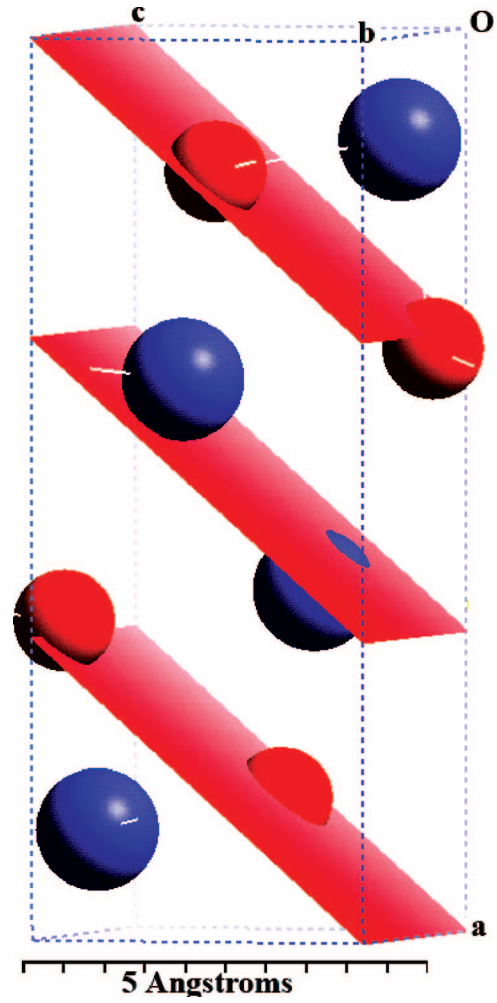

Figure 4. Unit cell of SnS, with Sn atoms colored blue and S atoms colored red. The (301) planes are shown for reference.

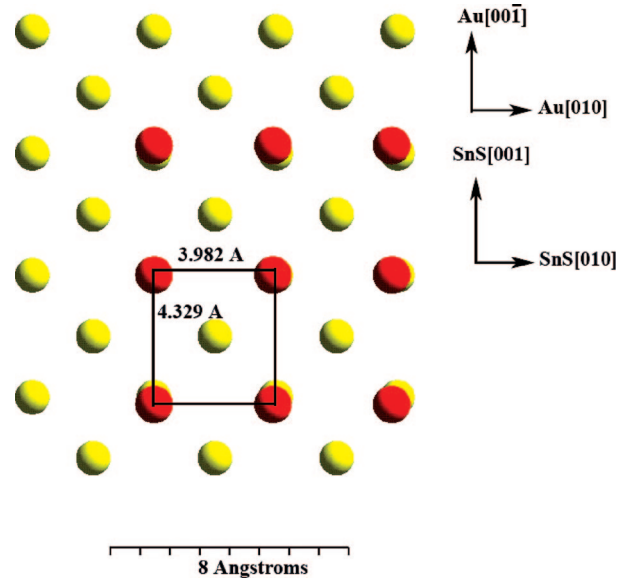

Figure 5. Interface model for SnS(100) on Au(100). The Au atoms are colored yellow, and the S atoms are colored red. On the SnS(100) plane, the spacing between adjacent sulfur atoms is 3.982 Å in the [010] direction and 4.329 Å in the [001] direction. The in-plane mismatch is −2.4% in the [010] direction and +6.1% in the [001] direction.

atoms in the [010] direction is 3.982 Å, and in the [10$\bar{3}$] direction the distance alternates between 8.437 and 8.701

(41) Lefebvre, I.; Szymanski, M. A.; Olivier-Fourcade, J.; Jumas, J. C. *Phys. Rev. B* **1998**, *58*, 1896.

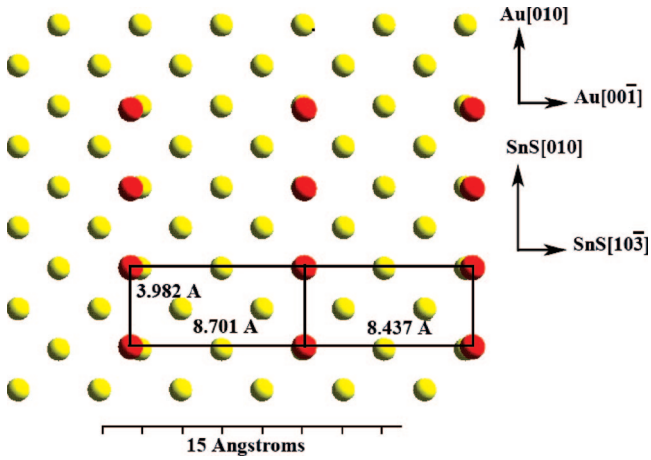

Figure 6. Interface model for SnS(301) on Au(100). The Au atoms are colored yellow, and the S atoms are colored red. The mismatch in the [010] direction is −2.4%, and in the [10$\bar{3}$] direction the mismatch alternates between +3.4% and +6.7%. In the [10$\bar{3}$] direction the lattice mismatch was calculated by comparing the spacing between the S atoms (i.e., 8.347 and 8.701 Å) with a doubled Au unit mesh (i.e., 2 × 4.079 Å).

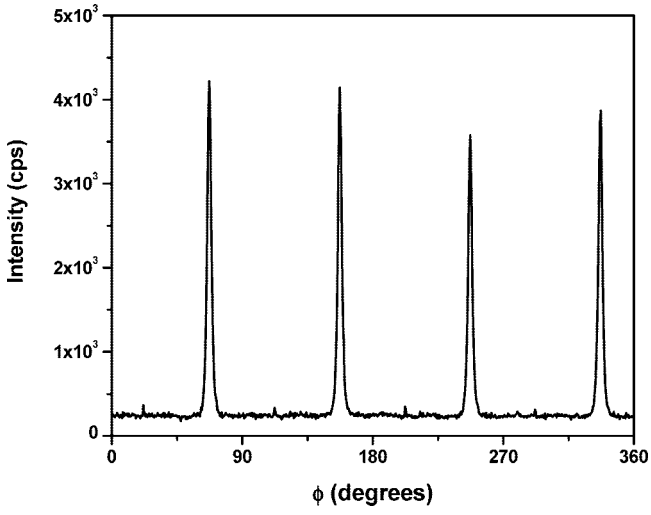

Figure 7. Azimuthal scans for (210) reflection of SnS. The azimuthal scans were obtained by setting 2θ equal to the angle of maximum diffracted intensity for the (201) reflection ($2\theta = 27.48°$) and tilting the sample to the angle χ corresponding to the angle between the (201) and (100) planes ($\chi = 54.5°$ for SnS). The four peaks in the azimuthal scan are separated by 90°. The average fwhm of the peaks is 3.16°.

Å. The mismatch in the [010] direction is −2.4%, and in the [10$\bar{3}$] direction the mismatch alternates between +3.4% and +6.7%. In the [10$\bar{3}$] direction the lattice mismatch was calculated by comparing the spacing between the S atoms (i.e., 8.347 and 8.701 Å) with a doubled Au unit mesh (i.e., 2 × 4.079 Å). Hence, although the lattice mismatch is similar for the [100] and [301] orientations, the [100] orientation is energetically preferred because it provides a larger number of coincidence points per unit area than the [301] orientation.

The quality of the epitaxial SnS nanostructure can be obtained by X-ray azimuthal scans and X-ray rocking curves. An azimuthal scan is a cross section of a pole figure at a tilt angle χ which corresponds to the maximum intensity of the reflections in the pole figure. Figure 7 shows an azimuthal scan for the (210) reflections of SnS at a tilt angle of 54.5°. The expected 4-fold symmetry is observed for the SnS

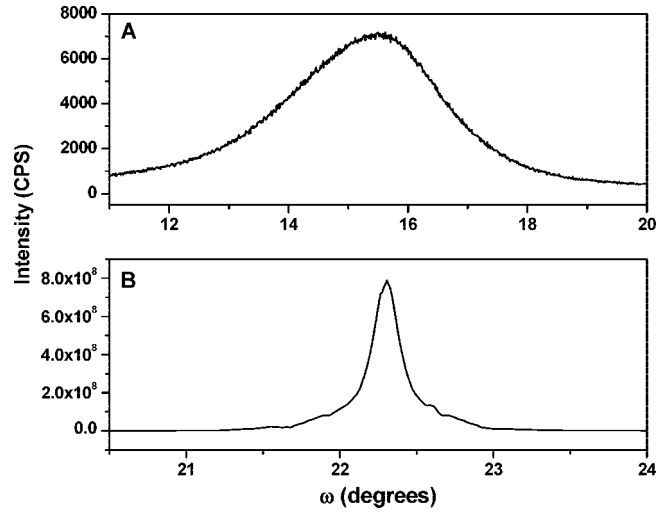

Figure 8. X-ray rocking curves for (A) SnS(400)/(301) and (B) Au(200). The fwhm is 2.9° for SnS(400)/(301) and 0.23° for Au(200).

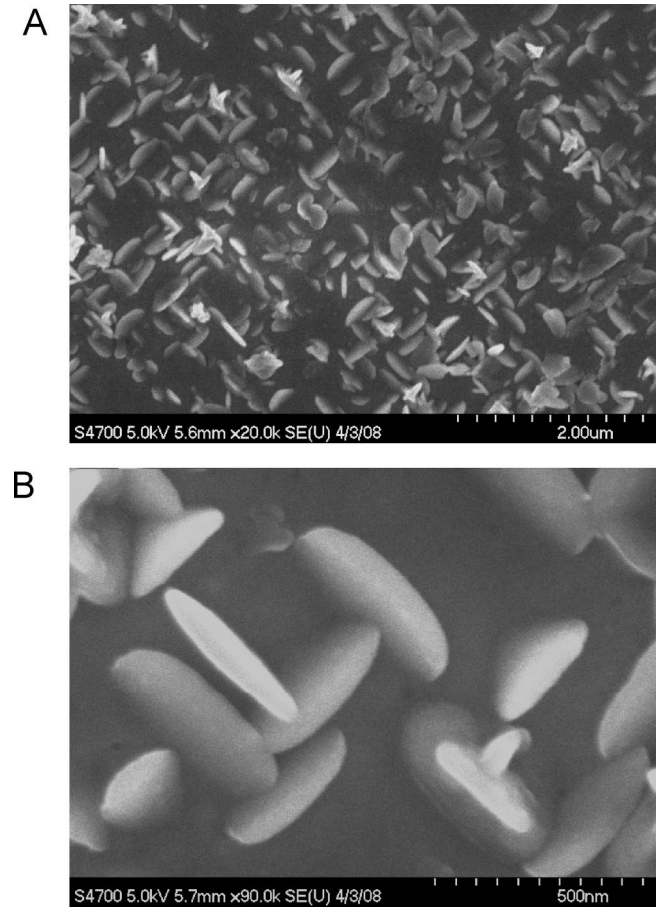

Figure 9. SEM micrographs of an epitaxial deposit of SnS nanodisks on Au(100) at low (A) and high (B) magnifications.

deposit and the substrate. The average full width at half-maximum (fwhm) of SnS is 3.16°. The average peak intensity of SnS relative to the background is 16:1, indicating that SnS has a [100] orientation with little or no fiber texture. If the deposit had a fiber texture, the ratio between the average peak intensity and the background would be 1:1. Parts A and B of Figure 8 show the X-ray rocking curves of SnS(400)/(301) and Au(200). The fwhm's of SnS(400)/(301) and Au(200) are 2.9° and 0.23°, respectively. These results

indicate that SnS has predominately a [100] out-of-plane orientation with a 2.9° mosaic spread.

Scanning electron micrographs of SnS electrodeposited with a cathodic current density of 3 mA/cm^2 are shown in Figure 9 at two different magnifications. The ratio Sn:S is approximately 1:1 when measured by energy-dispersive spectroscopy (EDS). The morphology of the SnS deposit has a disklike structure. The disks are approximately 300 nm in diameter and 50 nm in thickness. Because the XRD results show that the primary crystallographic orientation of the SnS is [100], the disks in the SEM image have the (100) edge of SnS in contact with the Au(100) surface.

Conclusions

Epitaxial SnS nanodisks are electrodeposited on a Au(100) single crystal using the cathodic deposition approach. The deposition solution was originally developed by Brownson et al.[19] The SnS deposit grows with two different out-of-plane orientations of [100] and [301]. The two orientations can be distinguished by X-ray pole figures. The quality of the SnS is analyzed by azimuthal and rocking curve scans. The rocking curve shows that the film has a 2.9° mosaic spread. EDS also confirms a 1:1 Sn:S ratio. For photovoltaic and photoelectrochemical applications, it will be interesting in future work to deposit SnS on less expensive Au-sputtered glass which has a [111] orientation. It will also be interesting to deposit epitaxial SnS/Si and SnS/InP heterojunctions.

Acknowledgment. This work was supported by NSF Grant DMR-0504715.

CM801502M